

# PACOX: A FPGA-based Pauli Composer Accelerator for Pauli String Computation

Tran Xuan Hieu Le, Tuan Hai Vu, Vu Trung Duong Le, Hoai Luan Pham and Yasuhiko Nakashima

**Abstract**—Pauli strings are a fundamental computational primitive in hybrid quantum-classical algorithms. However, classical computation of Pauli strings suffers from exponential complexity and quickly becomes a performance bottleneck as the number of qubits increases. To address this challenge, this paper proposes the Pauli Composer Accelerator (PACOX), the first dedicated FPGA-based accelerator for Pauli string computation. PACOX employs a compact binary encoding with XOR-based index permutation and phase accumulation. Based on this formulation, we design a parallel and pipelined processing element (PE) cluster architecture that efficiently exploits data-level parallelism on FPGA. Experimental results on a Xilinx ZCU102 FPGA show that PACOX operates at 250 MHz with a dynamic power consumption of 0.33 W, using 8,052 LUTs, 10,934 FFs, and 324 BRAMs. For Pauli strings of up to 19 qubits, PACOX achieves speedups of up to 100 times compared with state-of-the-art CPU-based methods, while requiring significantly less memory and achieving a much lower power-delay product. These results demonstrate that PACOX delivers high computational speed with superior energy efficiency for Pauli-based workloads in hybrid quantum-classical systems.

**Index Terms**—quantum computing, Pauli string, FPGA, SoC

## I. INTRODUCTION

IN recent years, the rapid development of hybrid quantum-classical algorithms [1], [2] has intensified the demand for efficient classical processing of quantum operators [3]–[5]. Pauli strings are widely used in Hamiltonian simulation [6], variational quantum algorithms [7], and quantum error correction [8], [9]. For the development of quantum algorithms, researchers have used software packages such as Qiskit SparsePauliOp [10] and PennyLane Pauli [11]. However, in many practical workloads, the dominant computational cost arises from repeated Pauli string computations [12]. At large  $n$ , these operations quickly become a bottleneck due to the exponential growth of the operator space [13], [14].

Numerous studies aim to improve computational speed and support larger values of  $n$ . The tree-based method in [15] reduces arithmetic operations and allows moderately sized problems to run on a single node with limited memory, but it is limited to  $n \leq 15$ . L. Hantzko *et al.* [16] avoid expensive matrix multiplications by computing Pauli weights recursively using matrix slicing, yet their method supports only  $n \leq 10$ . T. Kurita *et al.* [17] proposed an efficient algorithm to group Pauli

This research was supported by the VNUHCM - University of Information Technology's Scientific Research Support Fund. Corresponding author: Tuan Hai Vu (Email: haivt@uit.edu.vn).

Tran Xuan Hieu Le, Vu Trung Duong Le, Hoai Luan Pham, and Yasuhiko Nakashima are with Nara Institute of Science and Technology, 8916-5 Takayama-cho, Ikoma, Nara 630-0192, Japan.

Tuan Hai Vu is with University of Information Technology, Ho Chi Minh City, 700000, Vietnam, and Vietnam National University, Ho Chi Minh City, 700000, Vietnam.

strings and reduce measurement cost in variational quantum eigensolver algorithms. Although this approach supports larger  $n$ , it requires a large amount of memory.

Another emerging trend is the use of graphics processing units (GPUs) for Pauli string computation. In particular, the `apply_pauli_rotation` function in cuQuantum [18] is optimized for NVIDIA GPU architectures [19]. In this context, Huang *et al.* [20] proposed a novel approach to improve Pauli string synthesis by incorporating architecture-aware optimization strategies. Furthermore, Y. Teranishi *et al.* [21] introduced a parallel expectation value computation (EVC) method based on out-of-order qubit reordering and optimized Pauli-string scheduling. Although these GPU-based approaches provide significant performance improvements, the authors also reported scalability limitations as  $n$  increases, which remains a major challenge for supporting larger quantum systems.

To overcome software limitations, many quantum systems have been developed on hardware platforms, especially using Field-Programmable Gate Arrays (FPGAs). FPGAs are widely used in quantum-classical systems because they support low-latency quantum control, real-time signal processing, and quantum emulation tasks [22]–[25]. Additionally, the work presented in [26] proposed a method to address memory and computational challenges encountered in quantum emulation. However, existing FPGA-based approaches primarily focus on quantum control or circuit-level emulation and do not directly address Pauli string computation, which involves exponential index transformations and phase composition.

To the best of our knowledge, **this work is the first to propose a dedicated FPGA accelerator for Pauli string computation itself**. This paper proposes PACOX (PAuli COnposer X Accelerator, where “X” is a phonetic shorthand for “accelerator”), an FPGA-based design for fast Pauli string computation built upon the Pauli Composer (PC) algorithm [27], which addresses the performance limitations of software-based implementations through three key innovations: (1) an optimized memory organization that efficiently manages context data and Pauli matrix storage to support exponential data growth in a hardware-friendly manner, (2) a parallel and pipelined FPGA architecture that exploits data-level parallelism, and (3) a compact binary encoding of Pauli strings that reformulates operator evaluation as XOR-based index permutation and phase accumulation. Together, these design choices enable an efficient and hardware-oriented solution for Pauli string computation.

## II. IMPROVED PACOX ALGORITHM

**Algorithm 1** PACOX algorithm

```

Require: Pauli string  $\mathbf{x}$ 
1:  $n \leftarrow |\mathbf{x}|, L \leftarrow 2^n$ 
2:  $n_Y \leftarrow$  number of  $Y$  matrices in  $\mathbf{x}$ 
3:  $\mathbf{k} \leftarrow \underbrace{[0, \dots, 0]}_{2^n}, \mathbf{m} \leftarrow \mathbf{k}.copy$ 
4:  $\mathbf{v} \leftarrow [\tilde{V}[x_{n-1}] \dots \tilde{V}[x_0]]$  in base 2  $\{\tilde{V} = [1, 1, 0, 0]\}$ 
5:  $\mathbf{k}[0] \leftarrow [\tilde{X}[x_{n-1}] \dots \tilde{X}[x_0]]$  in base 10  $\{\tilde{X} = [0, 1, 1, 0]\}$ 
6:  $\mathbf{m}[0] \leftarrow (-i)^{n_Y \bmod 4}$ 
7: for  $l \in [0, \dots, n-1]$  do
8:   [parallel with  $N$  {PEp}]  $\{p = 0, 1, \dots, N-1\}$ 
9:    $s_p \leftarrow L/N \times p$ 
10:   $e_p \leftarrow L/N \times (p+1) - 1$ 
11:   $\mathbf{k}[L+s_p : L+e_p] \leftarrow \mathbf{k}[s_p : e_p] + (-1)^{\tilde{X}[x[l]]} L$ 
12:   $\mathbf{m}[L+s_p : L+e_p] \leftarrow \mathbf{m}[s_p : e_p] \oplus \neg \mathbf{v}[l]$ 
13: end for
14: return A sparse matrix stacking  $(\mathbf{k}, \mathbf{m})$ 

```

The Pauli matrices are Hermitian, Unitary, and together with the identity matrix they form the set  $\sigma_{0,1,2,3} = \{I, X, Y, Z\}$ . Given an  $n$ -qubit string  $\mathbf{x} \in \{0, 1, 2, 3\}^n$ , we construct the operator through tensor product ( $\otimes$ ):

$$P(\mathbf{x}) := \sigma_{x_{n-1}} \otimes \sigma_{x_{n-2}} \otimes \dots \otimes \sigma_{x_0}, \quad (1)$$

which is known as the basic computation in various optimization problems such as Variational Quantum Eigensolver, Quantum Approximate Optimization Algorithm, and Quadratic Unconstrained Binary Optimization. Let  $P_{j,k}(\mathbf{x})$  denote the matrix elements of  $P(\mathbf{x})$  ( $j, k \in [0, \dots, 2^n - 1]$ ). Native tensor product returns  $P(\mathbf{x})$  as  $2^n \times 2^n$  matrix, which consumes massive memory for even small  $n$ . Luckily, the operator  $P$  has been proved in [27] that for each row  $j$ , there exists exactly one element at column  $k[j]$  such that  $P_{j,k[j]}(\mathbf{x}) = \pm 1$ . Consequently, the problem reduces to determining vector  $\mathbf{k}$  and the sign of the  $2^n$  nonzero entries associated with  $\mathbf{x}$ . The sequential algorithm has been proposed therein; hence, the computational complexity of the original algorithm is lower bounded by  $2^n$ . Therefore, we present a parallel version in Algorithm 1, in which the red lines indicate the key improvements introduced over the PC algorithm. At each iteration  $l$ , the algorithm applies sign inversions and index shifts on  $\{\mathbf{k}, \mathbf{m}\}$ , which made the bottleneck of the whole algorithm because their size increases exponentially ( $2^n$ ) based on the number of qubits  $n$ . Hence, using  $N$  data-parallel PEs, the above operations are faster than  $N$  times. Note that  $N$  must be a power of 2, then  $L/N$  returns the valid index. Furthermore, we replace multiplication by the XOR operator, which reduces a lot of cycles overall.

Figure 1 illustrates the data flow of the PACOX algorithm implemented with 32 PEs ( $N = 32$ ). The initial data vectors  $(\mathbf{k}, \mathbf{m})$ , which consist of  $L$  tuples  $(\mathbf{k}[i], \mathbf{m}[i])$ , are evenly partitioned into 32 segments. Each segment has a length of  $L/32$ . After partitioning, the data segments are streamed in a pipelined manner to their corresponding PEs for computation. In each PE, the arithmetic logic unit (ALU) independently updates the assigned  $(\mathbf{k}[i], \mathbf{m}[i])$  entries. The computed results are stored in local memory, which also holds the original input data. The updated results are then merged with the existing data to form the input for the next computation cycle, referred

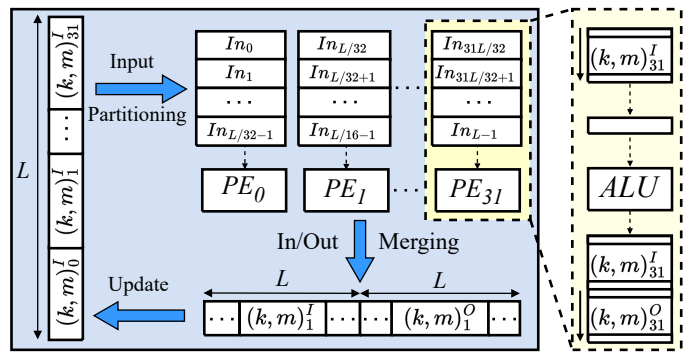


Fig. 1. Dataflow and internal datapath of PEs in PACOX method.

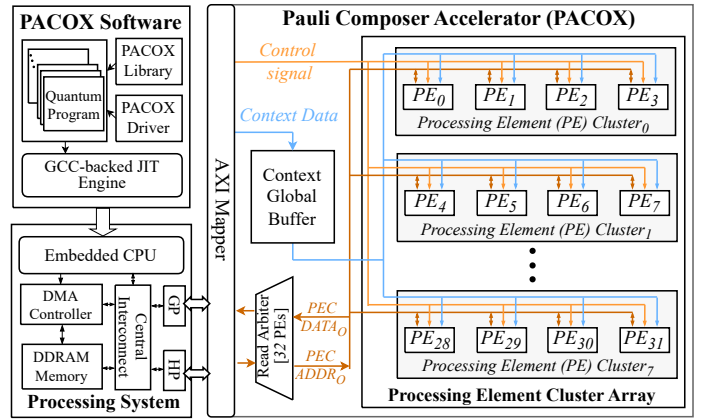


Fig. 2. Overview hardware architecture of PACOX.

to as *In/Out Merging*. By exploiting data-level parallelism with 32 PEs, repeated for  $l$  iterations, the execution time of this computation is reduced by approximately a factor of 32 compared to the sequential implementation.

### III. HARDWARE ARCHITECTURE

#### A. Overview

Figure 2 illustrates the system-level architecture of the proposed PACOX implemented on a system-on-chip (SoC) platform. The architecture consists of a processing system (PS) and programmable logic (PL). The PS runs GNU/Linux and provides application-level control across user and kernel spaces. In the user space, programmers define Context data structures that describe Pauli strings. These contexts are compiled in the kernel space by a GCC-based PACOX compiler and transferred to the programmable logic (PL) via the AXI bus using programmable input/output (PIO). As the control and configuration data are lightweight and transferred only once, a 64-bit PIO interface is sufficient. The PACOX hardware in the PL consists of four main modules: an AXI Mapper, a Context Global Buffer, a Read Arbiter, and a PE Cluster (PEC) Array. The AXI Mapper manages data communication between the PS and the local data memory of the PEs. Once the Context Global Buffer receives the configuration data from the PS, the PEC Array starts computing the vectors  $(\mathbf{k}, \mathbf{m})$ . Once the computation is finished, the PEC Array signals the PS, and the results  $\mathbf{k}$  and  $\mathbf{m}$  are fetched into DDR memory via the AXI Mapper and Read Arbiter using DMA.

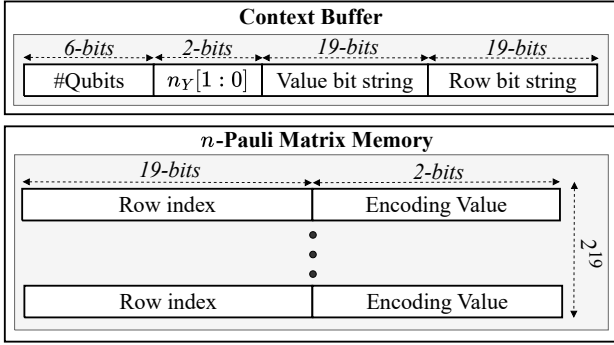


Fig. 3. Memory organization of PACOX.

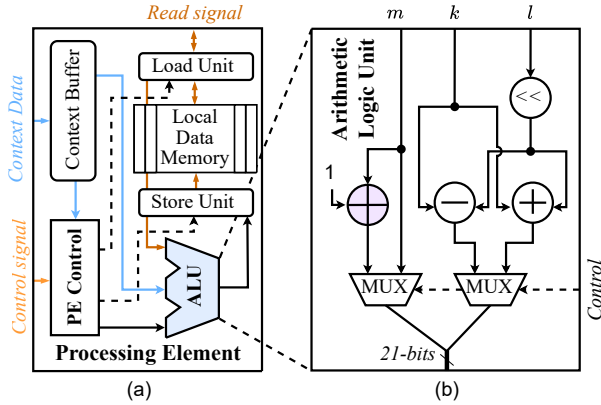


Fig. 4. Micro-architecture of the (a) PE and (b) ALU.

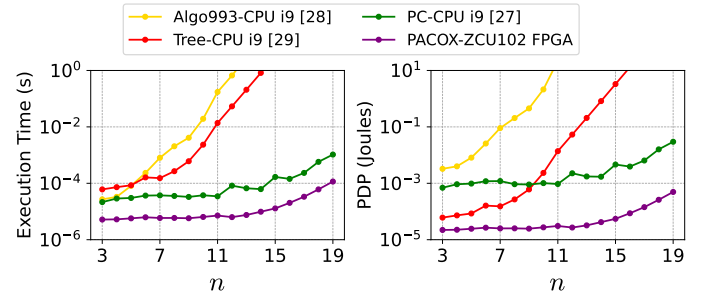
As discussed in Section II, the matrix size grows exponentially with the  $n$ , while FPGA platforms are limited by on-chip memory resources. Figure 3 shows the memory organization of the proposed PACOX design for efficient FPGA implementation. Two types of memory are used: Context Buffers and the  $n$ -Pauli Matrix Memory. The Context Buffers store context data and include a 6-bit signal that indicates the number of qubits supported by PACOX. In addition, the Context Buffer stores other configuration parameters, such as  $ny[1:0]$ , the Row bit string, and the Value bit string. The Row bit string is defined as  $[\bar{X}[x_{n-1}] \dots \bar{X}[x_0]]_2$ , while the Value bit string is given by  $[\bar{V}[x_{n-1}] \dots \bar{V}[x_0]]_2$ . The  $n$ -Pauli Matrix Memory is the largest memory component and is used to store the vectors  $(\mathbf{k}, \mathbf{m})$ . To support up to  $n = 19$ , this memory requires a depth of  $2^{19}$ . When the  $n$ -Pauli Matrix Memory is implemented on FPGA platforms with more abundant BRAM resources, such as the Xilinx Alveo or Versal series, PACOX can be scaled to support larger values of  $n$ .

#### B. High-performance Processing Element and ALU

To match the 128-bit width of the DMA bus, four PEs are grouped into a single cluster, enabling the simultaneous readout of four output data items per transfer. Based on the available resources of the ZCU102 platform, the PACOX architecture is configured with a total of 32 PEs organized into a PEC array, corresponding to eight PECs. Figure 4a illustrates the architecture of an individual PE. Each PE incorporates a Context Buffer to reduce fan-in and fan-out overhead during

TABLE I  
PACOX DESIGN UTILIZATION ON THE ZCU102 FPGA  
(POST-IMPLEMENTATION).

Design Name	Freq. (MHz)	Resources			Power (W)
		LUTs	FFs	BRAM	
AXI Mapper		322	252	0	0.005
Read Arbiter		127	574	0	0.001
Context Buffer	250	0	1886	0	0.0292
Cluster Array		7603	8222	324	0.2948
<b>PACOX (Total)</b>	<b>250</b>	<b>8052</b>	<b>10934</b>	<b>324</b>	<b>0.33</b>

Fig. 5. Comparison of Execution Time and PDP for random  $n$ -qubit Pauli strings: PACOX vs. PC [27], Algo993 [28] and Tree [29] methods.

data transmission from PS to PE control logic. In addition to the basic logic blocks responsible for synchronization and pipelined computation across PEs, a Local Data Memory (LDM) is introduced. The LDM stores a vector of size  $2^{14}$ , where each entry is a tuple  $(\mathbf{k}[i], \mathbf{m}[i])$ . Here,  $\mathbf{k}[i]$  is a 19-bit integer, and  $\mathbf{m}[i]$  is a 2-bit integer encoding values from 0 to 3, corresponding to  $[1, -1, 1j, -1j]$ . Figure 4b shows the architecture of the ALU. It accepts three inputs, namely  $\mathbf{k}$ ,  $\mathbf{m}$ , and  $\mathbf{l}$ , and produces an output tuple  $(\mathbf{k}, \mathbf{m})$ . In this design, conventional multiplication operations are replaced by XOR-based logic enabled by the proposed binary encoding of Pauli strings. This replacement significantly reduces computational complexity and hardware cost compared with arithmetic multiplication. Owing to the simplicity of the ALU design, all computations are completed within a single clock cycle.

## IV. EXPERIMENTS AND RESULTS

To realize the proposed PACOX architecture shown in Fig. 2, the design was synthesized and implemented on the Xilinx ZCU102 FPGA platform using Vivado Design Suite version 2021.2. The synthesis and implementation processes employed the `Flow_areaOptimized_high` and `Performance_ExtraTimingOpt` strategies, respectively, to achieve a balanced trade-off between logic utilization, timing closure, and power efficiency. Table I summarizes the post-implementation resource utilization and power consumption of the PACOX design, with a breakdown across its major functional modules. The PACOX architecture uses 8,052 LUTs, 10,934 FFs, and 324 Block RAMs while operating at 250 MHz. Despite the high operating frequency and extensive on-chip memory usage, dynamic power consumption is

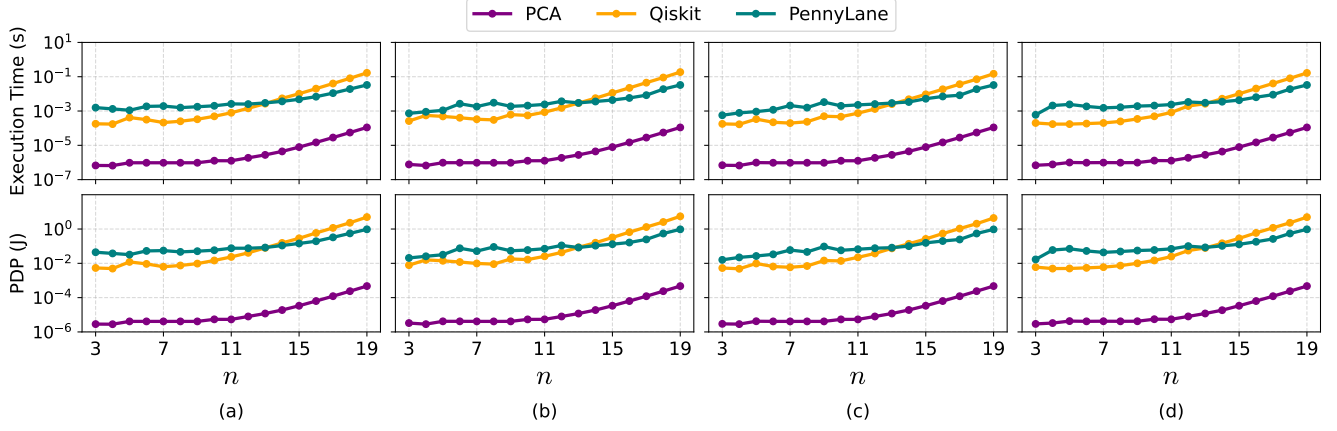


Fig. 6. Execution times for computing  $n$ -qubit Pauli string on the (a) Two-local [30], (b) VQE [31], (c) TFIM [32] and (d) Stabilizer code [33] testcases.

limited to 0.33 W, demonstrating good energy efficiency and compatibility with the target FPGA platform.

Figure 5 compares execution time and power-delay product (PDP) for different computing platforms with  $n = 3, 4, \dots, 19$ . All CPU experiments are conducted on an Intel i9-10940X processor running at 3.30 GHz. Within the measured range, PACOX consistently outperforms all CPU-based approaches in terms of execution time. Compared with the PC algorithm, PACOX demonstrates clear speedup across all evaluated problem sizes. This advantage becomes even more evident when compared with the **Algo993** [28] and **Tree** [29] methods, which exhibit rapidly increasing execution time as  $n$  grows. To conclude, this highlights PACOX’s superior performance in both execution time and energy efficiency, making it a promising solution for large-scale computations compared to conventional CPU-based methods.

We further compare the proposed PACOX with widely used CPU-based quantum software libraries on standard testcases, including Qiskit [10] and PennyLane [11]. Figure 6 shows the execution time for computing  $n$ -qubit Pauli strings on the Two-local [30], VQE [31], TFIM [32], and Stabilizer code [33] datasets with qubit counts ranging from 3 to 19. Across all test cases, PACOX consistently outperforms Qiskit and PennyLane, and the performance gap widens as the  $n$  increases. This highlights the effectiveness of the proposed hardware architecture for accelerating practical Pauli-based workloads. Figure 6 also reports the measured PDP for PACOX and the CPU-based libraries over the same qubit range. The PACOX achieves significantly lower PDP values across all datasets, demonstrating that its performance gains are obtained with superior energy efficiency.

## V. CONCLUSION

This paper presents PACOX, a dedicated FPGA-based architecture for accelerating Pauli string computation in hybrid quantum-classical systems. PACOX employs a compact binary encoding that transforms the entire process into an XOR-based index permutation and phase accumulation, enabling efficient parallel and pipelined execution on an FPGA. Implemented on a Xilinx ZCU102 platform, PACOX achieves up to two orders of magnitude speedup over representative CPU-based Pauli

computation methods, while significantly reducing memory usage and power consumption. These results demonstrate that PACOX provides a high-speed and energy-efficient hardware solution for accelerating Pauli-based quantum workloads.

## APPENDIX: USE CASE OF PACOX

In this section, we introduce several problems which are benchmarked in Fig. 6.

**Two-local Pauli strings.** These operators describe nearest-neighbor interactions such as  $XX$ ,  $YY$ , and  $ZZ$  in many fundamental Hamiltonians, including spin-chain models used in variational quantum algorithms. They are expressed as

$$P_j^x = I^{\otimes j} \otimes \sigma_x \sigma_x \otimes I^{\otimes(n-j-2)}, \quad x \in \{X, Y, Z\}.$$

**Stabilizer Code.** The Pauli string  $Z_j = I^{\otimes j} \otimes Z \otimes I^{\otimes(n-j-1)}$  is a basic element of the stabilizer generator  $\mathbb{P} = \{Z_0, \dots, Z_n\}$ . The observable  $\langle Z_0 \rangle$  also serves as a basic measurement observable.

**Variational Quantum Eigensolver (VQE).** We use the Hamiltonian of the LiH molecule with atomic coordinates  $[[0, 0, 0], [0, 0, 1.6 \text{ \AA}]]$  in the STO-3G basis. The Pauli strings are expressed as the sum

$$H_{\text{LiH}} = -7.3147I^{\otimes 4} + \dots + 0.0843Z_2Z_3.$$

**Transverse-Field Ising Model (TFIM).** The TFIM is a paradigmatic quantum spin model that captures the competition between nearest-neighbor Ising interactions and a transverse magnetic field. Its Hamiltonian is also given by the sum of Pauli strings

$$H_{\text{Ising}} = -J \sum_{j=1}^{N-1} Z_j Z_{j+1} - h \sum_{j=1}^N X_j,$$

where  $Z_j Z_{j+1}$  represents the nearest-neighbor Ising interaction, and  $X_j$  denotes the transverse-field term. In this work, the external field  $h$  is turned on.

We measure the evaluation time from initialization until obtaining the sparse matrix stacking of  $\{P_j^x\}$ ,  $\mathbb{P}$ ,  $H_{\text{LiH}}$ , or  $H_{\text{Ising}}$ . For larger problem instances, we increase the number of qubits or spin orbitals.

## REFERENCES

- [1] M. B. A. Dastagir and D. Han, "Towards Hybrid Quantum-Classical Deep Learning Architecture for Indoor-Outdoor Detection Using QCNN-LSTM and Cluster State Signal Processing," *IEEE Signal Processing Letters*, vol. 31, pp. 2945–2949, 2024.
- [2] I. Nikoloska and O. Simeone, "Training Hybrid Classical-Quantum Classifiers via Stochastic Variational Optimization," *IEEE Signal Processing Letters*, vol. 29, pp. 977–981, 2022.
- [3] Y. Alexeev, M. H. Farag, T. L. Patti, M. E. Wolf, N. Ares, A. Aspuru-Guzik, S. C. Benjamin, Z. Cai, S. Cao, C. Chamberland *et al.*, "Artificial intelligence for quantum computing," *Nature Communications*, vol. 16, no. 1, p. 10829, 2025.
- [4] A. Carrera Vazquez, C. Tornow, D. Riste, S. Woerner, M. Takita, and D. J. Egger, "Combining quantum processors with real-time classical communication," *Nature*, vol. 636, no. 8041, pp. 75–79, 2024.
- [5] A. Montanaro, "Quantum algorithms: an overview," *npj Quantum Information*, vol. 2, no. 1, pp. 1–8, 2016.
- [6] C. Sanavio, E. Mauri, and S. Succi, "Explicit Quantum Circuit for Simulating the Advection–Diffusion–Reaction Dynamics," *IEEE Transactions on Quantum Engineering*, vol. 6, pp. 1–12, 2025.
- [7] M. Cerezo, A. Arrasmith, R. Babbush, S. C. Benjamin, S. Endo, K. Fujii, J. R. McClean, K. Mitarai, X. Yuan, L. Cincio *et al.*, "Variational quantum algorithms," *Nature Reviews Physics*, vol. 3, no. 9, pp. 625–644, 2021.
- [8] E. Campbell, "A series of fast-paced advances in quantum error correction," *Nature Reviews Physics*, vol. 6, no. 3, pp. 160–161, 2024.
- [9] G. Dauphinais, D. W. Kribs, and M. Vasmer, "Stabilizer formalism for operator algebra quantum error correction," *Quantum*, vol. 8, p. 1261, 2024.
- [10] A. Javadi-Abhari, M. Treinish, K. Krsulich, C. J. Wood, J. Lishman, J. Gacon, S. Martiel, P. D. Nation, L. S. Bishop, A. W. Cross, B. R. Johnson, and J. M. Gambetta, "Quantum computing with Qiskit," 2024.
- [11] V. Bergholm, J. Izaac, M. Schuld, C. Gogolin, S. Ahmed, V. Ajith, M. S. Alam, Alonso-Linaje *et al.*, "Pennylane: Automatic differentiation of hybrid quantum-classical computations," *arXiv preprint*, vol. arXiv:1811.04968, 2018.
- [12] M. Kohda, R. Imai, K. Kanno, K. Mitarai, W. Mizukami, and Y. O. Nakagawa, "Quantum expectation-value estimation by computational basis sampling," *Physical review research*, vol. 4, no. 3, p. 033173, 2022.
- [13] O. Crawford, B. van Straaten, D. Wang, T. Parks, E. Campbell, and S. Brierley, "Efficient quantum measurement of Pauli operators in the presence of finite sampling error," *Quantum*, vol. 5, p. 385, 2021.
- [14] G. Lami and M. Collura, "Nonstabilizerness via perfect pauli sampling of matrix product states," *Physical Review Letters*, vol. 131, no. 18, p. 180401, 2023.
- [15] O. Koska, M. Baboulin, and A. Gazda, "A tree-approach Pauli decomposition algorithm with application to quantum computing," in *ISC High Performance 2024 Research Paper Proceedings (39th International Conference)*. Prometheus GmbH, 2024, pp. 1–11.
- [16] L. Hantzko, L. Binkowski, and S. Gupta, "Tensorized Pauli decomposition algorithm," *Physica Scripta*, vol. 99, no. 8, p. 085128, 2024.
- [17] T. Kurita, M. Morita, H. Oshima, and S. Sato, "Pauli string partitioning algorithm with the Ising model for simultaneous measurements," *The Journal of Physical Chemistry A*, vol. 127, no. 4, pp. 1068–1080, 2023.
- [18] H. Bayraktar, A. Charara, D. Clark, S. Cohen, T. Costa, Y.-L. L. Fang, Y. Gao, J. Guan, J. Gunnels, A. Haidar *et al.*, "cuQuantum SDK: A High-Performance Library for Accelerating Quantum Science," in *2023 IEEE International Conference on Quantum Computing and Engineering (QCE)*, vol. 1. IEEE, 2023, pp. 1050–1061.
- [19] M. Osama, D. Thanos, and A. Laarman, "Parallel Equivalence Checking of Stabilizer Quantum Circuits on GPUs," in *International Conference on Tools and Algorithms for the Construction and Analysis of Systems*. Springer, 2025, pp. 109–128.
- [20] Q. Huang, D. Winderl, A. Meijer-Van De Griend, and R. Yeung, "Redefining Lexicographical Ordering: Optimizing Pauli String Decompositions for Quantum Compiling," in *2024 IEEE International Conference on Quantum Computing and Engineering (QCE)*, vol. 1. IEEE, 2024, pp. 885–896.
- [21] Y. Teranishi, S. Hiraoka, W. Mizukami, M. Okita, and F. Ino, "Lazy Qubit Reordering for Accelerating Parallel State-Vector-based Quantum Circuit Simulation," *ACM Transactions on Quantum Computing*, vol. 6, no. 4, pp. 1–33, 2025.
- [22] X. Qin, W. Zhang, L. Wang, Y. Zhao, Y. Tong, X. Rong, and J. Du, "An FPGA-based hardware platform for the control of spin-based quantum systems," *IEEE Transactions on Instrumentation and Measurement*, vol. 69, no. 4, pp. 1127–1139, 2019.
- [23] U. Baek, Y. Xu, G. Huang, L. Doolittle, and I. Siddiqi, "An FPGA-based quantum feedback system for real-time qubit control," *Bulletin of the American Physical Society*, vol. 64, 2019.
- [24] T. H. Vu, V. T. D. Le, H. L. Pham, Y. Nakashima *et al.*, "QEA: An Accelerator for Quantum Circuit Simulation with Resources Efficiency and Flexibility," in *2025 10th IEEE International Conference on Integrated Circuits, Design, and Verification (ICDV)*. IEEE, 2025, pp. 55–60.
- [25] A. Giorgio, "Project and Implementation of a Quantum Logic Gate Emulator on FPGA Using a Model-Based Design Approach," *IEEE Access*, vol. 12, pp. 41 317–41 353, 2024.
- [26] P. H. Luan, V. T. Hai, Y. Nakashima *et al.*, "Theoretical Analysis of the Memory-Efficient Matrix Storage Method for Quantum Emulation Accelerators with Gate Fusion on FPGAs," in *2024 IEEE 17th International Symposium on Embedded Multicore/Many-core Systems-on-Chip (MCSOC)*. IEEE, 2024, pp. 366–373.
- [27] S. Vidal Romero and J. Santos-Suárez, "PauliComposer: compute tensor products of Pauli matrices efficiently," *Quantum Information Processing*, vol. 22, no. 12, p. 449, Dec 2023.
- [28] P. L. Fackler, "Algorithm 993: Efficient computation with kronecker products," *ACM Transactions on Mathematical Software (TOMS)*, vol. 45, no. 2, pp. 1–9, 2019.
- [29] I. Selesnick and C. Burrus, "Automatic generation of prime length FFT programs," *IEEE Transactions on Signal Processing*, vol. 44, no. 1, pp. 14–24, 1996.
- [30] M. A. Nielsen and I. L. Chuang, *Quantum computation and quantum information*. Cambridge university press, 2010.
- [31] A. Peruzzo, J. McClean, P. Shadbolt, M.-H. Yung, X.-Q. Zhou, P. J. Love, A. Aspuru-Guzik, and J. L. O'brien, "A variational eigenvalue solver on a photonic quantum processor," *Nature communications*, vol. 5, no. 1, p. 4213, 2014.
- [32] S. Sachdev, *Quantum Phase Transitions*, 2nd ed. Cambridge University Press, 2011.
- [33] D. Gottesman, *Stabilizer codes and quantum error correction*. California Institute of Technology, 1997.